OPEN

A quantitative study of chemical kinetics for the synthesis of doped oxide nanocrystals using FTIR

Na Zhang[1,2]*, Xin Wang[1]*, Zhizhen Ye[1] & Yizheng Jin[1,3]

[1]State Key Laboratory of Silicon Materials, Cyrus Tang Center for Sensor Materials and Applications, Department of Materials Science and Engineering, Zhejiang University, Hangzhou 310027, People's Republic of China, [2]Department of Chemistry, Zhejiang University, Hangzhou 310027, People's Republic of China, [3]Center for Chemistry of High-Performance and Novel Materials, Zhejiang University, Hangzhou 310027, People's Republic of China.

The synthesis of Mg-doped ZnO nanocrystals was employed as a model system to quantitatively study the chemical kinetics of the precursor conversion reactions at synthetic conditions and the correlations with the formation of doped nanocrystals. An accurate method using Fourier transform infrared spectroscopy was developed to explore the alcoholysis reactions of the cationic precursors. Our study showed that three independent factors, molar ratio of dopant precursor, reaction temperature and coordination ligands of cationic precursors influenced the relative reactivity of magnesium to zinc precursor, and in turn the formation of Mg-doped ZnO nanocrystals with defined shapes and properties. This understanding underpins the advancement of the syntheses of doped nanocrystals and should be useful for future rational design of new synthetic systems.

Colloidal semiconductor nanocrystals are intriguing materials due to the unique combination of rich solid state properties and remarkable solution dispersibility[1,2]. Recently the chemical mechanisms and kinetics of reactions behind the synthesis of colloidal semiconductor nanocrystals have attracted great attention[3–15]. A number of material systems, including CdSe, CdS, InP and InAs, were explored. The results suggested that the precursor conversion was the rate-limiting step in the formation of colloidal nanocrystals. Quantitative studies on the kinetics of the conversion reactions showed that the precursor reactivity played a critical role in terms of determining the size, size distribution and shape of the resulting nanocrystals.

Doping or alloying, a process chemically akin to doping, provides an effective approach to control the electronic structure of colloidal nanocrystals and bring in composition-dependent properties[16–19]. Doped, or alloyed nanocrystals may lead to functional materials with unprecedented properties, such as modified band structures, enhanced electrical conductivity and impressive emission properties[20–25]. Furthermore, recent studies showed that the incorporation of specific impurities into the host lattices not only altered the composition of the nanocrystals but also caused morphological changes[26–33]. For example, our group demonstrated the synthesis of Mg-doped ZnO nanocrystals and Cd-doped ZnO nanocrystals with controllable optical bandgaps and well-defined shapes, ranging from tetrapods to ultrathin nanowires[26,27].

For many doping systems, a key concept linking the growth of the doped nanocrystals and the kinetics of the associated reactions is balancing the relative reactivity of dopant to host precursor[19]. A few recent studies suggested to adjust the reactivity of the precursors by selecting appropriate coordinating ligands to achieve doped or alloyed nanocrystals[25,34–37]. For example, Milliron and coworkers found that for the synthesis of Al-doped ZnO nanocrystals, successful doping was achieved when zinc stearate and aluminum acetylacetonate were selected as precursors. No doping was observed when the dopant precursor was replaced by aluminum stearate which was less reactive[25]. For the synthesis of ternary alloyed CuInS$_2$ nanocrystals, copper fatty acid salts were too reactive in comparison to indium fatty acid salts. To this end, the less reactive copper thiolate was used to prevent the formation of Cu$_x$S nanophases[35].

Despite the perceived importance of balancing the relative reactivity of dopant to host precursor, the chemical kinetics of the precursor conversion reactions for doped nanocrystal systems have not been defined at a quantitative level. There is lack of complete understanding of how the critical factors, such as reaction temperature, influence the relative reactivity of dopant to host precursor and the formation of doped nanocrystals. As a

1

consequence, the choice of precursors and the selection of experimental parameters were based on empirical or qualitative rules and relied heavily on trial and error.

Here we employed the synthesis of Mg-doped ZnO nanocrystals as a model system to quantitatively study the chemical kinetics of the cationic precursors and to explore the relationship between the kinetics of the precursor conversion reactions and the formation of doped nanocrystals with defined properties and shapes. In the previous work, we show that the incorporation of Mg dopants into the ZnO seed crystals plays an important role in the primary growth stage, resulting in initial growth seeds having diverse crystallographic structures, which are critical for the generation of doped nanocrystals with different shapes[26]. In such a scenario, the chemical kinetics of the precursor conversion reactions is critical in terms of governing the deposition of Mg dopants on the host seed crystals during the initial growth stage, and therefore the shapes and the properties of the doped oxide products. To this end, an accurate experimental method based on Fourier transform infrared spectroscopy (FTIR) to measure the initial reaction rates of the alcoholysis reactions was developed. Important kinetic parameters of the precursor conversion reactions, such as activation energy were determined. The results revealed how the key factors, *i.e.* reaction temperature, molar ratio of dopant precursor and coordination ligands of cationic precursors influenced the relative reactivity of dopant to host precursor and, in turn, the formation of Mg-doped ZnO nanocrystals.

Results

The synthesis of Mg-doped ZnO nanocrystals was based on the alcoholysis of a zinc carboxylate salt and a magnesium carboxylate salt[26]. We used a reverse injection approach. In this approach, the solution containing the metal precursors was kept at a lower temperature, 150°C, prior to the injection into the reaction flask heated to a temperature between 260 and 300°C to start the alcoholysis reactions. The advantage of the reverse injection approach is better control over the reaction pathways by minimizing hydrolysis or other undesirable reactions of metal carboxylate salts which may take place at high temperatures. According to our experience, the reverse injection approach, a degasification procedure using liquid nitrogen trap and precise control over the reaction temperatures (within ±2.5°C) were important for achieving syntheses with decent reproducibility.

We found that for a given set of cationic precursors, magnesium stearate ($Mg(St)_2$) and zinc stearate ($Zn(St)_2$), the morphologies and properties of the Mg-doped ZnO nanocrystals were influenced by both the molar ratio of $Mg(St)_2$ in the cationic precursors and the reaction temperature (Fig. 1, S3 and S4). The properties of the doped oxide nanocrystals, including the optical bandgaps extracted from the corresponding UV-Visible absorption (UV-Vis) spectra (Fig. S3), the contents of magnesium dopant determined by inductively coupled plasma atomic emission spectroscopy (ICP-AES) measurements and the average diameters of the ultrathin nanowires or the arms of the branched nanocrystals measured by high resolution transmission electron microscope (HRTEM) analyses (Fig. S4) were summarized in Table 1. We suggest that the different contrast at the tips of the ultrathin nanowires in the TEM images is mainly due to volume effects[26]. This interpretation is supported by the energy-dispersive X-ray spectroscopy (EDS) mapping results revealing that no segregation of Mg rich domains within the nanocrystals (Fig. S5). As shown in Fig. 1 (middle column), for the reactions conducted at 250°C, the shape of the Mg-doped ZnO nanocrystals changed from branched nanocrystals, including tetrapods, tripods and bipods, to ultrathin nanowires when the ratio of $Mg(St)_2$ in the cationic precursors increased from 50 to 60 mol%. The higher molar ratio of magnesium precursor resulted in a larger optical bandgap, a higher

reaction temperature
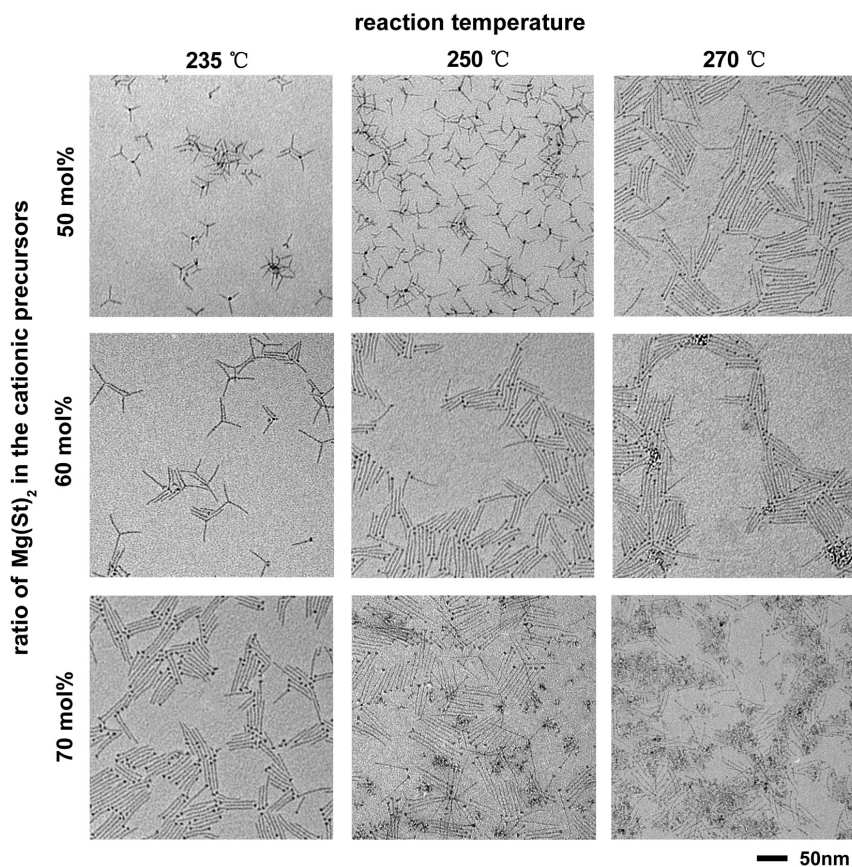
Figure 1 | **Typical TEM images of the oxide nanocrystals synthesized at various conditions.** $Zn(St)_2$ and $Mg(St)_2$ were employed as the zinc and magnesium precursors, respectively.

content of magnesium dopant and a smaller average diameter of the anisotropic oxide nanocrystals. Further increasing the ratio of $Mg(St)_2$ to 70 mol% led to the occurrence of irregular nanoparticles mixed with ultrathin nanowires. The occurrence of the irregular nanoparticles was due to the formation of oxide nanocrystals having cubic structure similar to that of bulk MgO. These results are in line with our previous report[26]. Remarkably, we observed temperature dependent shape evolution of the Mg-doped ZnO nanocrystals (Fig. 1, middle row). For the reactions starting with a fixed ratio, 60 mol%, of $Mg(St)_2$ in the cationic precursors, increasing the reaction temperature from 235 to 250°C resulted in morphological changes from branched nanocrystals, including tetrapods, tripods and bipods, to ultrathin nanowires. The higher reaction temperature of 250°C generated doped oxide nanocrystals with a larger optical bandgap, a higher content of magnesium dopant and a smaller average diameter. Further increasing the reaction temperature to 270°C led to products consisting of both ultrathin nanowires and irregular nanoparticles. These facts indicated that increasing the molar ratio of $Mg(St)_2$ in the cationic precursors or increasing the reaction temperature had similar effects on the formation of Mg-doped ZnO nanocrystals. This finding was confirmed by the following experiments. Three reactions (Fig. 1, diagonal) were conducted at conditions of 235°C and 70 mol% of $Mg(St)_2$, 250°C and 60 mol% of $Mg(St)_2$, and 270°C and 50 mol% of $Mg(St)_2$, respectively. All products from the three reactions consisted of exclusively ultrathin nanowires with almost identical properties in terms of the optical bandgaps (3.88 eV), the contents of magnesium dopant (30.2–30.9 at.%) and the average diameters (2.0 nm), as shown in Table 1. Therefore synergetic modifications on both the molar ratio of $Mg(St)_2$ in the cationic precursors and the reaction temperature may result in Mg-doped ZnO nanocrystals with almost identical properties.
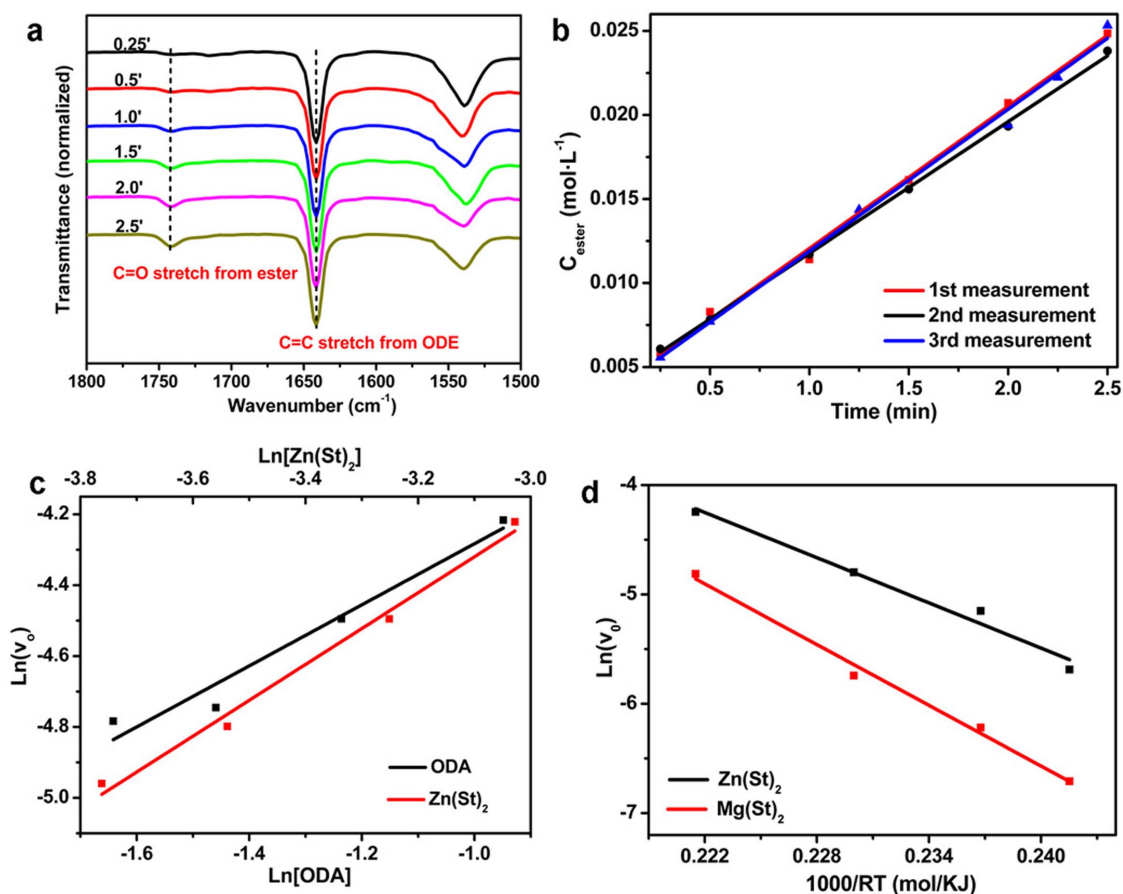
The chemical kinetics of the alcoholysis reactions for both $Zn(St)_2$ and $Mg(St)_2$ were investigated, aiming to explain the temperature dependent formation of the Mg-doped ZnO nanocrystals. FTIR was employed because ester, the by-product associated with the formation of the oxide nanocrystals, was readily detected by this technique (Fig. 2a)[26,38]. Special care on the experimental operations was taken to improve the accuracy for measuring the concentrations of ester in the reaction mixtures (refer to supporting information for details). Next a modified system was used for the determination of the initial reaction rates of the alcoholysis reactions. Additional free fatty acid (0.2 mmol), which readily converted the initially formed small oxide nanocrystals from the alcoholysis reactions back to metal carboxylate salts, was introduced into the reaction system. In this way, the amount of metal carboxylate salts was kept as constant before the free acid was consumed. Given that 1-octadecanol (ODA) was in large excess, typically less than 5% of ODA was consumed within the time of measurements which varied from 1.5 to 5.5 min depending on the reaction rates. Therefore, for a first order of approximation, the concentration of ODA was treated as a constant. The reaction rates were treated as constant values within the time of measurements. Hence the initial reaction rates were determined simply by interpreting the slope of the linear fitting curve from the C_{ester} - t plot. In general, linear curve fitting with a coefficient of determination (R^2) greater than 0.99 was achieved. The relative standard deviations of the initial reaction rates from three parallel measurements were in the rage of 1–9% (Fig. 2b). The kinetic parameters of the alcoholysis reactions, including reaction orders and activation energy were extracted using the initial reaction rates from sets of reactions with one variable. The results (Fig. 2c) showed that for the synthesis of ZnO nanocrystals using $Zn(St)_2$ and ODA as the reagents, the reaction orders for $Zn(St)_2$ and ODA were 1.01 and 0.86, respectively. The $ln(r)$ - $1000/(RT)$ plot shown in Fig. 2d indicated that the activation energy was 69 KJ mol^{-1}. In contrast, the activation energy for the alcoholysis reaction using $Mg(St)_2$ and ODA as the reagents was 87 KJ mol^{-1}.

The FTIR method was also used to quantitatively evaluate the reactivity of the cationic precursors with different coordination ligands. Three zinc fatty acid salts with different chain lengths, *i.e.* $Zn(St)_2$, zinc myristate ($Zn(My)_2$) and zinc decanoate ($Zn(De)_2$) were studied. For the reactions under the same reaction conditions (Fig. 3a), the initial ester formation rates followed the order of $Zn(St)_2$ (8.2 mmol L^{-1} min^{-1}) < $Zn(De)_2$ (9.8 mmol L^{-1} min^{-1}) < $Zn(My)_2$ (12.5 mmol L^{-1} min^{-1}). This order is different from that of the chain length of the carboxylate ions, St$^-$ > My$^-$ > De$^-$. We suggest that at least three factors, the interactions between the hydrocarbon chains, the steric hindrance of the carboxylate ions and the strengths of the metal-ligand bonds influence the reactivity of the zinc carboxylates. First, the interactions between the alkyl chains are critical for the stability of the reverse micelle structures of zinc carboxylates formed in the non-polar solvent, ODE. Stronger molecular interactions lead to more stable reverse micelle structures and in consequence lower reactivity. FTIR analyses on the zinc precursors at synthetic conditions showed that the asymmetric stretching bands of the -COO$^-$ groups were doublets for $Zn(De)_2$ and singlets for $Zn(My)_2$ and $Zn(St)_2$. According to Ellis's FTIR investigations on a series of solid state zinc fatty acid salts, the splitting of the absorption peaks was correlated with relative strengths of the zinc-carboxylate bonds and van der Waals interactions between hydrocarbon chains[39]. Therefore it is expected that the reverse micelle structures of $Zn(De)_2$ in ODE is relatively unstable compared with those of $Zn(St)_2$ or $Zn(My)_2$ in ODE. Second, when the carboxylate precursors undergo the nucleophilic attack by the alcohol, the effects of steric hindrance of the carboxylate ligands should be taken into

Table 1 | The properties of the Mg-doped ZnO nanocrystals synthesized under various conditions (corresponding to Fig. 1)

|	235°C	250°C	270°C
50 mol% of $Mg(St)_2$			
shape	branched nanocrystals	branched nanocrystals	nanowires
optical band gap (eV)	3.77	3.83	3.88
Mg content in NCs (at.%)		27.0	30.5
diameter (nm)		2.2 ± 0.3	2.0 ± 0.2
60 mol% of $Mg(St)_2$			
shape	branched nanocrystals	nanowires	nanowires and irregular particles
optical band gap (eV)	3.80	3.88	
Mg content in NCs (at.%)	23.8	30.2	
diameter (nm)	2.3 ± 0.3	2.0 ± 0.3	
70 mol% of $Mg(St)_2$			
shape	nanowires	nanowires and irregular particles	nanowires and irregular particles
optical band gap (eV)	3.88		
Mg content in NCs (at.%)	30.9		
diameter (nm)	2.0 ± 0.3		

Figure 2 | Chemical kinetics of the alcoholysis reactions studied by FTIR. (a) Temporal evolution of FTIR spectra recorded from an alcoholysis reaction. Reaction conditions: $Zn(St)_2$ 0.375 mmol, ODA 3.75 mmol, HSt 0.2 mol, ODE 10.2 g, temperature = 250°C. (b) Determination of the initial reaction rates. The initial formation rates of ester from the three measurements were 8.5 mmol L^{-1} min^{-1}, 7.9 mmol L^{-1} min^{-1} and 8.4 mmol L^{-1} min^{-1}, respectively. (c) Determination of the reaction orders for $Zn(St)_2$ and ODA from the plot of initial formation rate of ester versus the concentration of $Zn(St)_2$ and the plot of the initial formation rate of ester versus the concentration of ODA, respectively. (d) Irving plots of the initial reaction rates of the alcoholysis reactions. The reactions were carried out at 270, 250, 235 and 225°C respectively.

consideration. Shorter alkyl chains of the carboxylate salts lead to less steric effects, and in consequence higher reactivity. Third, the reactivity of zinc carboxylates depends on the strengths of the zinc-carboxylate bonds. Shorter alkyl chains of the carboxylate salts result in stronger interactions between the zinc ions and the carboxylate ligands and in turn lower reactivity. In short, the reactivity of the zinc fatty acid salts depends on the overall effects of the above three

factors and cannot be interpreted simply by the chain length of the carboxylate ions.

Discussion

The above results enlightened us to suggest that the formation of Mg-doped ZnO nanocrystals is largely controlled by the relative reactivity of magnesium to zinc precursor, which is influenced by three
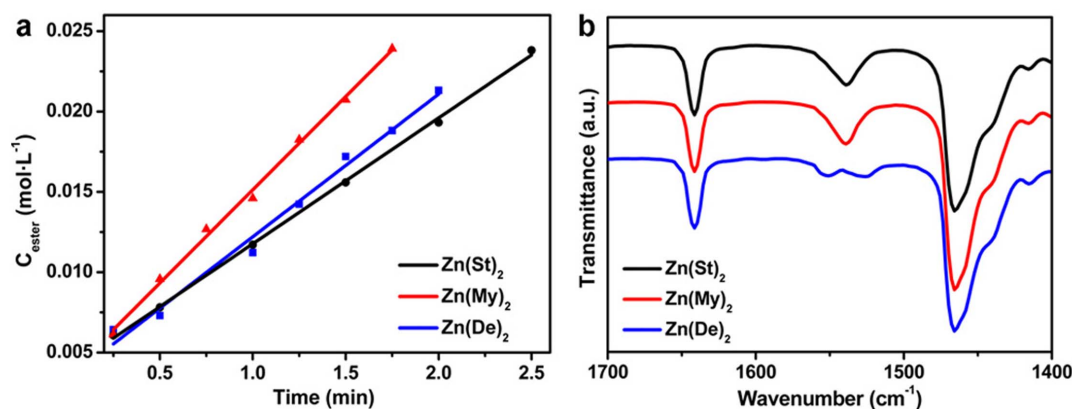
Figure 3 | (a) Initial reaction rates of the alcoholysis reactions for $Zn(St)_2$, $Zn(My)_2$ and $Zn(De)_2$, respectively. Reaction conditions: zinc carboxylate 0.375 mmol, ODA 3.75 mmol, the corresponding fatty acid 0.2 mmol, ODE 10.2 g, reaction temperature = 250°C. (b) FTIR spectra of the zinc carboxylates in ODE at 250°C.
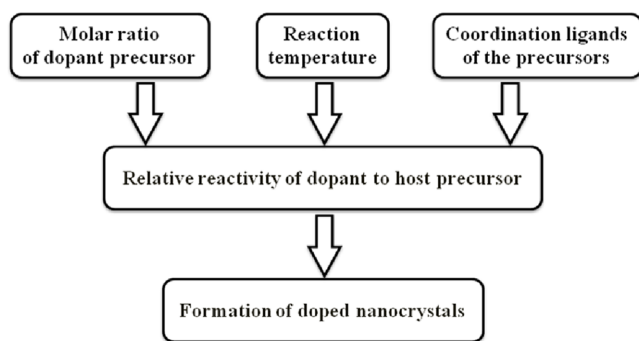
Figure 4 | Chemical kinetics of the precursor conversion reactions and the formation of doped nanocrystals.

independent factors, the molar ratio of dopant precursor, the reaction temperature and the coordination ligands of the cationic precursors (Fig. 4).

For a given set of dopant and host precursors and a fixed reaction temperature, the molar ratio of dopant precursor affects the relative reactivity of dopant to host precursor. The molar ratio of $Mg(St)_2$ in the cationic precursors is a key factor that modulates the synthesis of the Mg-doped ZnO nanocrystals.

Next we discuss the temperature dependent formation of the Mg-doped ZnO nanocrystals. The reactivity of each precursor is influenced by the reaction temperatures. Generally the temperature dependence of reactivity for one precursor is different from that for another precursor. In the case of $Mg(St)_2$ and $Zn(St)_2$, the activation energy for the alcoholysis reactions using $Mg(St)_2$ is higher than that using $Zn(St)_2$, suggesting that the temperature dependence of reactivity for $Mg(St)_2$ is more significant than that for $Zn(St)_2$. Hence the relative reactivity of magnesium to zinc precursor is influenced by the reaction temperature, causing temperature dependent formation of the Mg-doped ZnO nanocrystals (Fig. 1, middle row). For the reactions with a fixed 60 mol% of $Mg(St)_2$ in the cationic precursors, a balanced relative reactivity of dopant to host precursor was achieved at 250°C to generate ultrathin nanowires. At 270°C, $Mg(St)_2$ is relatively more active, resulting in the formation of products with mixed phases. At 235°C, the "effective" molar ratio of $Mg(St)_2$ is relatively smaller than that at 250°C, leading to the formation of branched nanocrystals rather than ultrathin nanowires.

The impact of coordination ligands on the reactivity of the precursors and the formation of doped nanocrystals was recognized by many research groups. Here we emphasize the importance of quantitatively interpreting the reactivity of the precursors. As shown by the quantitative FTIR measurements, the intrinsic reactivity of the three zinc carboxylates followed the order of $Zn(St)_2 < Zn(De)_2 < Zn(My)_2$, which was different from the order of the chain lengths. This fact was used to guide the synthesis of Mg-doped ZnO

nanocrystals with defined shapes and properties. For example, for the synthesis of Mg-doped ZnO ultrathin nanowires, when different zinc precursors and the same magnesium precursor, $Mg(St)_2$ were used, synergetic modifications on the ratio of the dopant precursor were required to achieve a balanced relative reactivity of dopant to host precursor. Our experiments showed that for the reactions conducted at 250°C, a ratio of 40, 30, and 35 mol% of $Zn(St)_2$, $Zn(My)_2$ and $Zn(De)_2$, respectively, led to the formation of ultrathin nanowires with almost identical properties (Fig. 5, S6, S7 and Table 2). These results agreed well with the predications from the FTIR measurements. We also conducted experiments by deliberately adding 0.2 mmol of HSt, HMy and HDe into the reactions starting with 40 mol% of $Zn(St)_2$, 30 mol% of $Zn(My)_2$, and 35 mol% of $Zn(De)_2$, respectively. The TEM (Fig. S8), UV-Vis spectra (Fig. S9), HRTEM (Fig. S10) and ICP-AES results (Table S1) show that additional ligands of free fatty acids do not influence the shape and the properties of the products.

In conclusion, we developed an accurate method using FTIR to measure the initial reaction rates of the alcoholysis reactions using metal carboxylates as the reagents. The measurements showed that the activation energy for the alcoholysis reactions using $Mg(St)_2$ and ODA, 87 KJ mol^{-1}, was higher than that for the reactions using $Zn(St)_2$ and ODA, 69 KJ mol^{-1}. In addition, the FTIR measurements revealed that the reactivity of three zinc fatty acid salts followed the order of $Zn(St)_2 < Zn(De)_2 < Zn(My)_2$, different from that of the chain length of the carboxylate ions. These results, together with the syntheses of oxide nanocrystals under various conditions, allowed us to conclude that the formation of Mg-doped ZnO nanocrystals was largely controlled by the relative reactivity of magnesium to zinc precursor, which was influenced by three independent factors, the molar ratio of dopant precursor, the reaction temperature and the coordination ligands of cationic precursors. The correlation between the reactivity of the precursors and the shape and properties of the doped oxide nanocrystals stems from the fact that the formation of the growth seeds, critical in terms of determining the shape and structure of the final products, is influenced by the incorporation of Mg dopants into the ZnO seed crystals at the initial growth stage, which is largely affected by the reaction rates of both the zinc precursor and magnesium precursor. The knowledge on the chemical kinetics of the precursor conversion reactions is beneficial in terms of guiding the selection of the precursors and the design of the experiments to obtain Mg-doped ZnO nanocrystals with targeted shapes and properties.

Our work provides an excellent example of correlating the chemical kinetics of precursor conversions to the formation of doped nanocrystals at a quantitative level. Considering that FTIR has been applied in many synthetic systems for oxide nanocrystals, such as the non-hydrolytic aminolysis approach[9,28,40–43], our method can be profitably utilized to quantitatively study the chemical kinetics of the precursor conversions reactions.
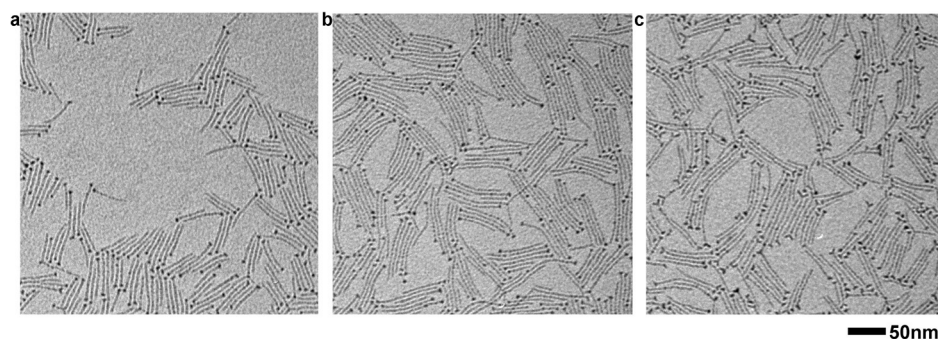
Figure 5 | (a)–(c) Typical TEM images of the Mg-doped ZnO ultrathin nanowires from the reaction starting with 40 mol% of $Zn(St)_2$, 30 mol% of $Zn(My)_2$ and 35 mol% of $Zn(De)_2$, respectively. The reactions were conducted at 250°C.

Table 2 | The properties of the Mg-doped ZnO nanocrystals synthesized with different zinc precursors (corresponding to Fig. 4)

	40 mol% of Zn(St)$_2$	30 mol% of Zn(My)$_2$	35 mol% of Zn(De)$_2$
optical band gap (eV)	3.88	3.88	3.88
Mg content in NCs (at.%)	30.2	30.0	30.8
diameter (nm)	2.0 ± 0.2	2.0 ± 0.3	2.0 ± 0.3

Methods

Materials. Zinc stearate (Zn(St)$_2$), magnesium stearate (Mg(St)$_2$), 1-octadecanol (ODA, 97%), methyl stearate (MSt, 99%), myristic acid (HMy, 98%), decanoic acid (HDe, 99%) and tetramethyl ammonium hydroxide (TMAH, 98%) were purchased from Alfa Aesar. 1-octadecene (ODE, tech 90%) was purchased from Acros Organics. Stearic acid (HSt, 97%) and zinc nitrate (Zn(NO$_3$)$_2$·6H$_2$O, 98%) were purchased from Aldrich. Ethyl acetate, toluene, chloroform, hexane, ethanol and methanol were analytical grade reagents purchased from Sinopharm Chemical. All chemicals were used as received.

Synthesis of Mg-doped ZnO nanocrystals. In all reactions, the cation quantity which was the total amount of the zinc precursor and the magnesium precursor was 0.5 mmol. The reactions were named after the molar ratio of the magnesium precursor in the cationic precursors. Typically, for a 60 mol% Mg(St)$_2$ reaction carried out at 250°C, ODA (2.5 mmol) and ODE (7.0 g) were loaded in a 50 mL three-necked flask, degassed and heated to 280°C under an argon flow. A separate solution of ODE (3.2 g) containing Zn(St)$_2$ (0.2 mmol) and Mg(St)$_2$ (0.3 mmol) at 150°C was rapidly injected into the reaction flask. The reaction temperature dropped to about 250°C and was kept at this temperature. When the reaction was finished, the reaction mixture was cooled to room temperature. The products were precipitated by a mixed solution of ethyl acetate and ethanol and collected by centrifugation. Next the nanocrystals were washed twice by using the combination of hexane/methanol and dispersed in nonpolar solvents such as toluene and hexane.

Initial reaction rates measured by FTIR. For a typical measurement, ODA (2.5 mmol) and ODE (7.0 g) were loaded into a 50 mL three-necked flask, degassed and heated to 280°C under an argon flow. A separate solution of ODE (3.2 g) containing Zn(St)$_2$ (0.5 mmol) and HSt (0.2 mmol) at 150°C was injected into the reaction flask. Aliquots (0.3 μL) taken by microsyringes at different time intervals were spread onto CaF$_2$ substrates to form smooth films with even thickness. These samples were used for FTIR analyses. The temporal concentrations of ester were calculated by integrating peak area using the C=C vibration bands of ODE at 1641 cm^{-1} as the references. Each sample were measured thrice to calculate the average values.

Characterization techniques, syntheses and characterizations of the zinc precursors (Fig. S1) and details of the method to determine the concentrations of ester in the reaction mixtures by FTIR (Fig. S2) were provided in the electronic supplementary information (SI).

1. Yin, Y. & Alivisatos, A. P. Colloidal nanocrystal synthesis and the organic-inorganic interface. *Nature* **437**, 664–670 (2005).
2. Talapin, D. V., Lee, J.-S., Kovalenko, M. V. & Shevchenko, E. V. Prospects of Colloidal Nanocrystals for Electronic and Optoelectronic Applications. *Chem. Rev.* **110**, 389–458 (2010).
3. Owen, J. S., Chan, E. M., Liu, H. & Alivisatos, A. P. Precursor Conversion Kinetics and the Nucleation of Cadmium Selenide Nanocrystals. *J. Am. Chem. Soc.* **132**, 18206–18213 (2010).
4. García-Rodríguez, R., Hendricks, M. P., Cossairt, B. M., Liu, H. & Owen, J. S. Conversion Reactions of Cadmium Chalcogenide Nanocrystal Precursors. *Chem. Mater.* **25**, 1233–1249 (2013).
5. Allen, P. M., Walker, B. J. & Bawendi, M. G. Mechanistic Insights into the Formation of InP Quantum Dots. *Angew. Chem. Int. Ed.* **49**, 760–762 (2010).
6. Xie, R., Li, Z. & Peng, X. Nucleation Kinetics vs Chemical Kinetics in the Initial Formation of Semiconductor Nanocrystals. *J. Am. Chem. Soc.* **131**, 15457–15466 (2009).
7. Li, Z., Ji, Y., Xie, R., Grisham, S. Y. & Peng, X. Correlation of CdS Nanocrystal Formation with Elemental Sulfur Activation and Its Implication in Synthetic Development. *J. Am. Chem. Soc.* **133**, 17248–17256 (2011).
8. Thomson, J. W., Nagashima, K., Macdonald, P. M. & Ozin, G. A. From Sulfur–Amine Solutions to Metal Sulfide Nanocrystals: Peering into the Oleylamine–Sulfur Black Box. *J. Am. Chem. Soc.* **133**, 5036–5041 (2011).
9. Jin, Y., Yi, Q., Ren, Y., Wang, X. & Ye, Z. Molecular mechanism of monodisperse colloidal tin-doped indium oxide nanocrystals by a hot-injection approach. *Nanoscale Res. Lett.* **8**, 153 (2013).
10. Ludi, B., Suess, M. J., Werner, I. A. & Niederberger, M. Mechanistic aspects of molecular formation and crystallization of zinc oxide nanoparticles in benzyl alcohol. *Nanoscale* **4**, 1982–1995 (2012).
11. Liu, H., Owen, J. S. & Alivisatos, A. P. Mechanistic Study of Precursor Evolution in Colloidal Group II—VI Semiconductor Nanocrystal Synthesis. *J. Am. Chem. Soc.* **129**, 305–312 (2007).
12. Hendricks, M. P., Cossairt, B. M. & Owen, J. S. The Importance of Nanocrystal Precursor Conversion Kinetics: Mechanism of the Reaction between Cadmium Carboxylate and Cadmium Bis(diphenyldithiophosphinate). *ACS Nano* **6**, 10054–10062 (2012).
13. Abe, S., Čapek, R. K., De Geyter, B. & Hens, Z. Tuning the Postfocused Size of Colloidal Nanocrystals by the Reaction Rate: From Theory to Application. *ACS Nano* **6**, 42–53 (2012).
14. Harris, D. K. & Bawendi, M. G. Improved Precursor Chemistry for the Synthesis of III-V Quantum Dots. *J. Am. Chem. Soc.* **134**, 20211–20213 (2012).
15. Guo, Y., Alvarado, S. R., Barclay, J. D. & Vela, J. Shape-Programmed Nanofabrication: Understanding the Reactivity of Dichalcogenide Precursors. *ACS Nano* **7**, 3616–3626 (2013).
16. Norris, D. J., Efros, A. L. & Erwin, S. C. Doped Nanocrystals. *Science* **319**, 1776–1779 (2008).
17. Peng, X. Band Gap and Composition Engineering on a Nanocrystal (BCEN) in Solution. *Acc. Chem. Res.* **43**, 1387–1395 (2010).
18. Regulacio, M. D. & Han, M. Y. Composition-Tunable Alloyed Semiconductor Nanocrystals. *Acc. Chem. Res.* **43**, 621–630 (2010).
19. Buonsanti, R. & Milliron, D. J. Chemistry of Doped Colloidal Nanocrystals. *Chem. Mater.* **25**, 1305–1317 (2013).
20. Pradhan, N., Goorskey, D., Thessing, J. & Peng, X. An Alternative of CdSe Nanocrystal Emitters: Pure and Tunable Impurity Emissions in ZnSe Nanocrystals. *J. Am. Chem. Soc.* **127**, 17586–17587 (2005).
21. Sarkar, S., Karan, N. S. & Pradhan, N. Ultrasmall Color-Tunable Copper-Doped Ternary Semiconductor Nanocrystal Emitters. *Angew. Chem. Int. Ed.* **50**, 6065–6069 (2011).
22. Cohn, A. W., Kittilstved, K. R. & Gamelin, D. R. Tuning the Potentials of "Extra" Electrons in Colloidal n-Type ZnO Nanocrystals via Mg^{2+} Substitution. *J. Am. Chem. Soc.* **134**, 7937–7943 (2012).
23. Kanehara, M., Koike, H., Yoshinaga, T. & Teranishi, T. Indium Tin Oxide Nanoparticles with Compositionally Tunable Surface Plasmon Resonance Frequencies in the Near-IR Region. *J. Am. Chem. Soc.* **131**, 17736–17737 (2009).
24. Della Gaspera, E. *et al.* Low-Temperature Processed Ga-Doped ZnO Coatings from Colloidal Inks. *J. Am. Chem. Soc.* **135**, 3439–3448 (2013).
25. Buonsanti, R., Llordes, A., Aloni, S., Helms, B. A. & Milliron, D. J. Tunable Infrared Absorption and Visible Transparency of Colloidal Aluminum-Doped Zinc Oxide Nanocrystals. *Nano Lett.* **11**, 4706–4710 (2011).
26. Yang, Y. *et al.* Dopant-Induced Shape Evolution of Colloidal Nanocrystals: The Case of Zinc Oxide. *J. Am. Chem. Soc* **132**, 13381–13394 (2010).
27. Wang, X. *et al.* Bandgap engineering and shape control of colloidal Cd$_x$Zn$_{1-x}$O nanocrystals. *Nanoscale* **5**, 6464–6468 (2013).
28. Jin, Y. *et al.* Synthesis and Characterization of Ultrathin Tin-Doped Zinc Oxide Nanowires. *Eur. J. Inorg. Chem.* **2012**, 4268–4272 (2012).
29. Wang, F. *et al.* Simultaneous phase and size control of upconversion nanocrystals through lanthanide doping. *Nature* **463**, 1061–1065 (2010).
30. Ding, Y., Gu, J., Ke, J., Zhang, Y.-W. & Yan, C.-H. Sodium Doping Controlled Synthesis of Monodisperse Lanthanide Oxysulfide Ultrathin Nanoplates Guided by Density Functional Calculations. *Angew. Chem. Int. Ed.* **50**, 12330–12334 (2011).
31. Wang, G., Peng, Q. & Li, Y. Lanthanide-Doped Nanocrystals: Synthesis, Optical-Magnetic Properties, and Applications. *Acc. Chem. Res.* **44**, 322–332 (2011).
32. Chen, D. *et al.* Modifying the Size and Shape of Monodisperse Bifunctional Alkaline-Earth Fluoride Nanocrystals through Lanthanide Doping. *J. Am. Chem. Soc.* **132**, 9976–9978 (2010).
33. Selishcheva, E., Parisi, J. & Kolny-Olesiak, J. Copper-assisted shape control in colloidal synthesis of indium oxide nanoparticles. *J. Nanopart. Res.* **14**, 711 (2012).
34. Zu, L., Wills, A. W., Kennedy, T. A., Glaser, E. R. & Norris, D. J. Effect of Different Manganese Precursors on the Doping Efficiency in ZnSe Nanocrystals. *J. Phys. Chem. C* **114**, 21969–21975 (2010).
35. Xie, R., Rutherford, M. & Peng, X. Formation of High-Quality I—III—VI Semiconductor Nanocrystals by Tuning Relative Reactivity of Cationic Precursors. *J. Am. Chem. Soc.* **131**, 5691–5697 (2009).
36. Ruberu, T. P. A. *et al.* Molecular Control of the Nanoscale: Effect of Phosphine–Chalcogenide Reactivity on CdS–CdSe Nanocrystal Composition and Morphology. *ACS Nano* **6**, 5348–5359 (2012).
37. Mikulec, F. V. *et al.* Organometallic Synthesis and Spectroscopic Characterization of Manganese-Doped CdSe Nanocrystals. *J. Am. Chem. Soc.* **122**, 2532–2540 (2000).
38. Chen, Y., Kim, M., Lian, G., Johnson, M. B. & Peng, X. Side Reactions in Controlling the Quality, Yield, and Stability of High Quality Colloidal Nanocrystals. *J. Am. Chem. Soc.* **127**, 13331–13337 (2005).

39. Taylor, R. A. & Ellis, H. A. Room temperature molecular and lattice structures of a homologous series of anhydrous zinc(II) n-alkanoate. *Spectrochimica Acta Part A* **68**, 99–107 (2007).

40. Zhang, Z., Zhong, X., Liu, S., Li, D. & Han, M. Aminolysis Route to Monodisperse Titania Nanorods with Tunable Aspect Ratio. *Angew. Chem. Int. Ed.* **44**, 3466–3470 (2005).

41. Cozzoli, P. D. *et al.* Colloidal Synthesis and Characterization of Tetrapod-Shaped Magnetic Nanocrystals. *Nano Lett.* **6**, 1966–1972 (2006).

42. Buonsanti, R. *et al.* Hyperbranched Anatase TiO_2 Nanocrystals: Nonaqueous Synthesis, Growth Mechanism, and Exploitation in Dye-Sensitized Solar Cells. *J. Am. Chem. Soc.* **133**, 19216–19239 (2011).

43. Buonsanti, R. *et al.* Nonhydrolytic Synthesis of High-Quality Anisotropically Shaped Brookite TiO_2 Nanocrystals. *J. Am. Chem. Soc.* **130**, 11223–11233 (2008).

Acknowledgments

Author contributions

J.Y. conceived and designed the experiments and wrote the manuscript. Z.N. and W.X. carried out the experiments. Y.Z. provided advices on the project. All authors reviewed the manuscript.

Additional information

Supplementary information accompanies this paper at http://www.nature.com/scientificreports

Competing financial interests: The authors declare no competing financial interests.

How to cite this article: Zhang, N., Wang, X., Ye, Z.Z. & Jin, Y.Z. A quantitative study of chemical kinetics for the synthesis of doped oxide nanocrystals using FTIR. *Sci. Rep.* **4**, 4353; DOI:10.1038/srep04353 (2014).